Repeat-Pass SAR Interferometry With Partially Coherent Targets

Daniele Perissin and Teng Wang

***Abstract*—By means of the permanent scatterer (PS) technique, repeated spaceborne synthetic aperture radar (SAR) images with relatively low resolution (about 25 m $\times$ 5 m for the European Remote Sensing (ERS) and Envisat satellites) can be used to estimate the displacement (1-mm precision) and 3-D location (1-m precision) of targets that show an unchanged electromagnetic signature. The main drawback of the PS technique is the limited spatial density of targets that behave coherently during the whole observation span (hundreds of PSs per square kilometer in urban site and up to few points in vegetated areas). In this paper, we describe a new approach for multitemporal analysis of SAR images that also allows extracting information from partially coherent targets. The basic idea is to loosen the restrictive conditions imposed by the PS technique. The results obtained in different test sites allowed to increase significantly the spatial coverage of the estimate of height and deformation trend, particularly in extraurban areas.**

***Index Terms*—Deformation monitoring, digital elevation models (DEMs), synthetic aperture radar interferometry (InSAR), time-series analysis.**

I. Introduction

SYNTHETIC aperture radar (SAR) interferometry (InSAR) [1] is a remote sensing technique that is able to recover high-resolution topographic profiles [2] (precision $\sim$10 m) and to highlight possible ground deformation phenomena [3] (precision $\sim$10 mm). Topography and movement of the illuminated terrain are extracted from interferograms, complex products of two scenes gathered at different times with different looking angles over the same area of interest. The main limitations of InSAR are temporal and geometrical decorrelations, caused by the variations of the ground's reflectivity as a function of time and of the incidence angle of data acquisition [4]. In addition, interferograms are also affected by the spatial variability of the water vapor content in the atmosphere [5].

Manuscript received March 28, 2010; revised December 3, 2010, March 18, 2011, and June 14, 2011; accepted June 19, 2011.

D. Perissin is with the Institute of Space and Earth Information Science, The Chinese University of Hong Kong (e-mail: daniele.perissin@cuhk.edu.hk).

T. Wang was with the State Key Laboratory for Information Engineering in Surveying, Mapping, and Remote Sensing, Wuhan University, Wuhan 430079, China, and also with the Dipartimento di Elettronica e Informazione, Politecnico di Milano, 20133 Milan, Italy (e-mail: wang.teng@gmail.com).

Color versions of one or more of the figures in this paper are available online at http://ieeexplore.ieee.org.

Digital Object Identifier 10.1109/TGRS.2011.2160644

The permanent scatterer (PS) technique [6], developed in Milan, Italy, at the "Politecnico di Milano" (POLIMI) toward the end of the 1990s, is a powerful multitemporal tool in the context of InSAR. By examining the pointlike radar targets which maintain their electromagnetic signature unchanged during the entire observation span, the PS technique allows to solve the well-known problems of interferometry. The PS technique has been widely applied with good results in a variety of cases, from ground deformation monitoring [7] to building stability analysis [8], and in recovering digital elevation models (DEMs) [9]. The PS technique presents an achievable accuracy of about 1 m in the height estimation of a target [10] and 1 mm in the estimate of the target displacement [11]. The main drawback of the PS approach is the low spatial density of permanent targets, and this is the case particularly outside of urbanized areas. Indeed, the lack of measurement points can be a considerable obstacle when monitoring with spaceborne SAR techniques. Different implementations of the PS technique have been developed by many research groups but without remarkable differences between them (from these, we recall [12]–[16]). Standing out from these groups are the researchers in Naples and in Stanford, who have proposed two multitemporal algorithms in an attempt to extract information from distributed targets. In the small baseline (SBAS) technique [17], the main concept is the analysis of interferograms with small normal baselines to reduce the geometrical decorrelation. The Stanford Method for PS (StaMPS) [18] is based essentially on the analysis of the phase's spatial and temporal correlation. By tracing and exploiting the clues left in the research path of the Naples and the Stanford groups, we have elaborated a new approach which loosens the strict conditions imposed by the PS technique. This innovative method which we present in this paper is able to extract information also from partially coherent targets and, hence, to increment the spatial distribution of measure points. We will name this approach, for the sake of simplicity, quasi-PS (QPS) technique. The proposed modifications, in relation to the original PS technique, can be summarized in the following three main points.

1) The images of the data set are no longer required to correlate with a unique common master image.
2) The target height and displacement are estimated by exploiting only an appropriate target-dependent subset of interferograms.
3) Spatial filtering is applied to enhance the signal-to-noise ratio of the interferometric phase of extended targets.

The three introduced concepts modify the kernel of the PS technique and allow to process also distributed and

decorrelating targets. From another standpoint, these modifications entail some loss of accuracy and resolution. In addition, the estimate of the terrain motion is limited to linear deformations. Therefore, when defining the study case, the QPS and PS techniques can be considered complementary approaches to be employed alternatively according to the imposing constraints and requirements.

The QPS approach has been used to analyze different test sites in nonurbanized areas, demonstrating its high potentiality. In particular, it was applied in the north of Italy to analyze Dossena, a small municipality located in a mountainous area in the Italian province of Bergamo. In this test site, it was possible to determine the borders of the active landslides around the inhabited area, covering also partially vegetated sections where no PS was present [19]. In addition, we report the results from two test sites in China. One is a newly built town located along the Yangtze River, upriver the Three Gorges Dam, an area around the Badong County, located in the extreme west of central China's Hubei Province (Enshi Prefecture). This is a town built on the steep riverbank, where potential landslides are likely to occur and need to be monitored, particularly after the area was flooded, with the operation of the Three Gorges Project beginning in 2003. The results obtained in this site, from QPS and StaMPS, are here submitted for comparison in order to highlight the different characteristics of the two techniques [20]. The other site that we report is the one around the Bashang prairie near Zhangbei, in the Hebei Province, where the QPS technique was used to perform topographic mapping, exposing its capability.

The main ideas presented in this paper were developed by the authors in POLIMI between the years 2005 and 2007 as many of the POLIMI group researchers were busy investigating multi-image InSAR processing. These researchers reached a variety of different results, among them, e.g., [11], [19], [30], [38], and [41]. In [29], for the first time, a general theoretical framework for processing long series of InSAR data was proposed, together with a Maximum Likelihood estimator for retrieving terrain height and deformation trend. The contribution that we give in this paper (of which the research stem began in the same context at POLIMI) is to present a simple technique to analyze long series of SAR images, one that requires only slight modifications of previous technologies in order to obtain an outstanding improvement of the results.

The QPS technique has been already used for a number of applications [39]. In particular, results obtained with this approach have been published in a Ph.D. thesis [40]. Currently, the QPS technique is incorporated in the SARPROZ InSAR processor, a software that is used for teaching and research purposes in the Institute of Space and Earth Information Science, The Chinese University of Hong Kong [42].

This paper is organized as follows. In Section II, we analyze the QPS algorithm, as an extension of the original PS technique. After a short introduction in which the main steps of the PS technique are evoked, we proceed by discussing the proposed modifications in Sections II-A–C. In Section III, we describe the results obtained in the processed data sets: Dossena, Badong, and Zhangbei in Sections III-A–C, respectively.

II. Algorithm

Next, we briefly turn our attention to some of the fundamental concepts of the PS technique, setting aside what is not needed for the immediate understanding of this paper. For a more exhaustive overview, interested readers can refer to [6] and [21].

Let us denote with s_i the ith complex SAR image (with $i = 1, \ldots, N$). The interferogram between the images i and k can thus be expressed as $I^{i,k} = s_i \cdot \ s_k^*$. Taking target p_0 as the reference point, the interferometric phase $\Delta\phi^{i,k}_{p,p_0} = \angle I^{i,k}_{p,p_0}$ of target p depends on its geometrical location as well as on its displacement, atmospheric disturbances, and noise [6]. In particular, the terms that depend on the target p height $\Delta h_{p,p_0}$ and linear deformation trend $\Delta v_{p,p_0}$ are expressed, respectively, by

$$\Delta\phi^{i,k}_{H,p,p_0} = \frac{4\pi}{\lambda}\frac{1}{R\sin\theta}\Delta h_{p,p_0} B^{i,k}_n \tag{1}$$

$$\Delta\phi^{i,k}_{D,p,p_0} = \frac{4\pi}{\lambda}\Delta v_{p,p_0} B^{i,k}_t \tag{2}$$

where $B^{i,k}_n$ is the interferometric normal baseline, $B^{i,k}_t$ is the temporal baseline, λ is the radar wavelength, θ is the looking angle, and R is the sensor–target distance.

In the standard PS technique, the target height and velocity are estimated by maximizing the absolute value of ξ_p [6] (we omit index p_0 to lighten the notation)

$$(\Delta\hat{h}_p, \Delta\hat{v}_p) = \arg\left\{\max\left(|\xi_p|\right)\right\} \tag{3}$$

where

$$\xi_p = \frac{1}{M}\sum_{(i,k)} e^{j\left(\Delta\phi^{i,k}_p - \Delta\phi^{i,k}_{H,p} - \Delta\phi^{i,k}_{D,p}\right)}. \tag{4}$$

In (4) (M is the number of pairs i, k), the following terms can be highlighted.

1) $\Delta\phi^{i,k}_p$ is the acquired interferometric phase (compensated for the terms that can be otherwise estimated, e.g., flat terrain).
2) $\Delta\phi^{i,k}_{H,p}$ is the elevation-dependent term given by (1).
3) $\Delta\phi^{i,k}_{D,p}$ is the deformation-trend-dependent term given by (2).

The maximum of the absolute value of (4) $\hat{\xi}_p = \max(|\xi_p|)$ is called temporal coherence, and it can be expressed as a function of the dispersion σ_ϕ of the phase residuals $\hat{\xi}_p \simeq e^{-\sigma^2_\phi/2}$ [21]. The variances of the height estimate and the deformation trend ($\sigma^2_{\Delta h}$ and $\sigma^2_{\Delta v}$, respectively) depend on the phase dispersion, the number of interferograms M, and the lever arm given by the corresponding acquisition parameter (normal- and temporal-baseline dispersions $\sigma^2_{B_n}$ and $\sigma^2_{B_t}$). More precisely, as derived in [21], we can approximate them with the following relations:

$$\sigma^2_{\Delta h} \simeq \left(\frac{\lambda R\sin\theta}{4\pi}\right)^2 \frac{\sigma^2_\phi}{M\sigma^2_{B_n}} \tag{5}$$

$$\sigma^2_{\Delta v} \simeq \left(\frac{\lambda}{4\pi}\right)^2 \frac{\sigma^2_\phi}{M\sigma^2_{B_t}}. \tag{6}$$

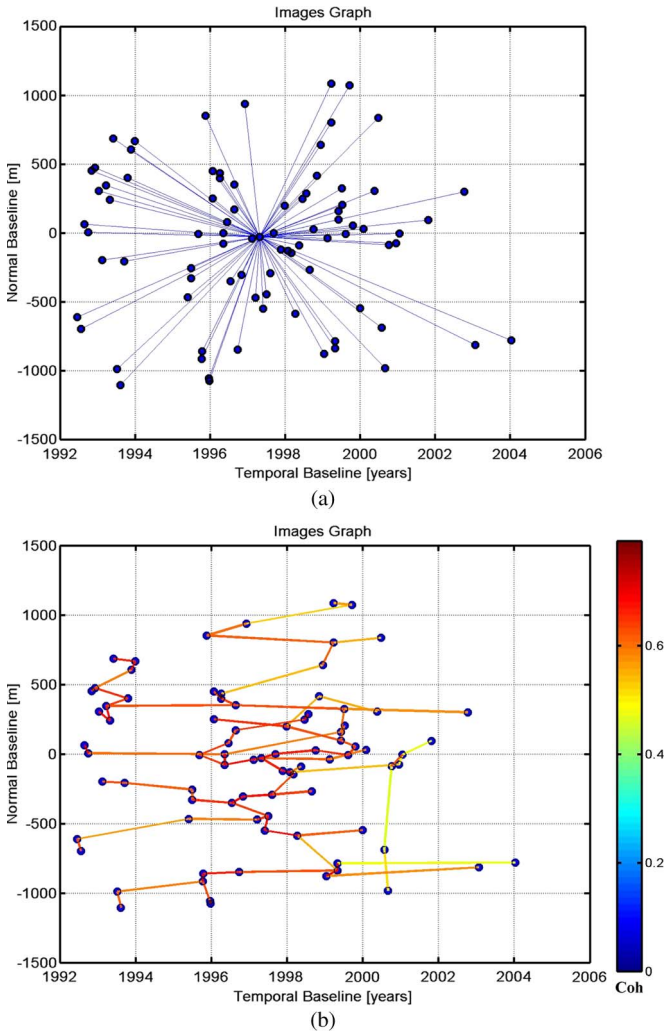

Fig. 1. Dossena data-set image graph. (a) Star graph, adopted in the PS technique. (b) MST graph, obtained by maximizing the average coherence. The color of the connections in (b) indicates the estimated coherence of the corresponding interferograms.

Normally, when considering the orbital tubes of the European Space Agency (ESA) satellites ERS and Envisat, the minimum number of images to perform successfully a PS analysis is about 20. The minimum temporal coherence to consider a target as a PS, by an available low number of images, is 0.9. When instead a higher number of images (more than 60) are processed, this figure decreases to 0.7. Under these conditions, the accuracy of the estimate can reach 1 m for the height [9] and 1 mm/year for the deformation trend [11].

A. Images' Graph

In the original PS analysis [6] (as well as in StaMPS [18]), the interferometric phase (4) is generated by referring all images to a common master acquisition. In the normal-baseline–temporal-baseline space, this configuration can be represented with a star graph as in Fig. 1(a), where each point (node) indicates an image and each connection (link) indicates an interferogram in the Dossena data set. In this framework, the graph connectivity assures the temporal continuity of the deformation measurements and, thus, the possibility of unwrapping the phase time series (and detecting nonlinear motions [23]). Moreover, the dispersions of normal and temporal baselines allow high-precision estimates of height and deformation trend. However, the main drawback of this combination is to make the assumption that each image can coherently interfere with the master acquisition, something that happens only for point-like targets. Now, we would like to discuss possible different choices for the graph that connects the images of the data set under study and the criteria to choose it, which is similar to what has been done in [24] but for different purposes.

We can single out three principal properties to describe an image's graph. The first one is connectivity: A graph is connected whenever, for all distinct pairs of nodes, a linking path exists. This property is needed in order to unwrap the phase time series. The second one is the number of links. Assuming that we are exploiting all the available N images (no isolated nodes), the minimum number of links in a graph is $N/2$ (or $(N+1)/2$ if N is odd), the minimum number to guarantee connectivity is $N-1$, and the number of links to make a complete graph (each node is connected with all others) is $N(N-1)/2$. Whenever the number of links is $> N-1$, we can say that the graph is redundant (given a pair of nodes, more linking paths exist). For the third and final one, we assign a weight to each link in order to quantify its goodness and to compare different graphs (e.g., with the average goodness of all links).

Since links correspond to interferograms, the interferometric coherence is the most appropriate index to characterize them. The coherence is defined as the normalized cross-correlation coefficient between two images i and k [27]

$$\gamma^{i,k} = \frac{E\left[s_i s_k^*\right]}{\sqrt{E\left[|s_i|^2\right] E\left[|s_k|^2\right]}} \tag{7}$$

where * is the complex conjugate operator and $E\{\cdot\}$ is the mathematical expectation.[1]

Different noise sources are at the origin of decorrelation in SAR interferograms [4], [28]. For this paper, we highlight two main phenomena: the geometric and temporal decorrelations. In the first one, the reflectivity of the terrain changes as a function of the look angle, and in the second one, it changes as a function of time. Assuming distributed random scattering and an exponential temporal decay, the phenomena can be simply modeled [24]–[26], and the absolute value of the coherence assumes the following form:

$$\gamma^{i,k} \simeq \gamma_{\text{geo}}^{i,k}\gamma_{\text{temp}}^{i,k} = \left(1-\left|\frac{B_n^{i,k}}{B_{n,c}}\right|\right)\text{rect}\left(\frac{B_n^{i,k}}{2B_{n,c}}\right)e^{-\left|B_t^{i,k}/B_{t,c}\right|} \tag{8}$$

where $B_{n,c}$ is the critical normal baselines, $B_{t,c}$ is a temporal decay constant (we can name it as critical temporal baseline), and $\text{rect}()$ is the rectangular function in the domain $-1/2$, $1/2$. The model could also be generalized by taking into account possible Doppler and carrier frequency diversity (as done in [22] for finite-dimension PSs).

[1]Here and in the following, to lighten the notation, we avoid writing explicitly the phase compensation for a known terrain model.

The geometric critical baseline can be expressed as a function of the system range resolution ρ and the terrain slope α [25]

$$B_{n,c} = \frac{\lambda R \tan(\theta - \alpha)}{2\rho} \tag{9}$$

and thus, the geometric decorrelation depends on the local topography of the analyzed area. Similarly, the temporal critical baseline depends on the typology and magnitude of the observed terrain motion [35]. This is why, in order to tune the model (8), we need *a priori* information on the area of interest. If *a priori* information is not available, the coherence must be directly estimated.

A cost-effective direct estimate of the coherence can be carried out on just a subset of N_p suitable points in the scene. The coherence of point p is calculated by means of spatial averages over an appropriate neighborhood $\mathrm{win}(p)$ of point p

$$\gamma_p^{i,k} = \frac{\sum\limits_{\mathrm{win}(p)} s_i s_k^*}{\sqrt{\sum\limits_{\mathrm{win}(p)} |s_i|^2 \sum\limits_{\mathrm{win}(p)} |s_k|^2}}. \tag{10}$$

The amplitude of the interferogram coherence is then retrieved by averaging the absolute value of the coherence of all N_p points

$$\gamma^{i,k} \simeq \frac{1}{N_p} \sum_p \left| \gamma_p^{i,k} \right|. \tag{11}$$

Either by exploiting a model as (8) or by estimating the coherence with (11), we are able to characterize each link of the graph. Finally, we assign descriptive numbers to the whole graph. In this way, it is possible to compare different graphs not only from a topological point of view but also quantitatively. Since the coherence is a normalized index, the sum of the link values can be interpreted as the effective number of interferograms in the graph used to estimate the height and the deformation trend

$$M_{\mathrm{eff}} = \sum_{(i,k)} |\gamma^{i,k}|. \tag{12}$$

Similarly, we can calculate the effective variances of normal and temporal baselines

$$\sigma^2_{B_{n\,\mathrm{eff}}} = \frac{\sum\limits_{(i,k)} |\gamma^{i,k}| \left| B_n^{i,k} \right|^2}{\sum\limits_{(i,k)} |\gamma^{i,k}|} \qquad \sigma^2_{B_{t\,\mathrm{eff}}} = \frac{\sum\limits_{(i,k)} |\gamma^{i,k}| \left| B_t^{i,k} \right|^2}{\sum\limits_{(i,k)} |\gamma^{i,k}|}. \tag{13}$$

The effective quantities of the graph (12) and (13) allow derivation of the average precision of the height estimate and the deformation trend, i.e., (5) and (6).

With the described parameters, we are able to compare different graphs and to choose the one that best fits the estimate requirements. If we intend to maximize the information to be extracted, then the optimum choice would be the complete graph. However, computational constraints can be an impediment when implementing the estimate. Moreover, the links of a complete graph are not necessarily all informative. In [24], the use of a minimum spanning tree (MST) is suggested, built by maximizing the modeled coherence of the links. The MST-generated image graph of the Dossena data set is shown in Fig. 1(b). The inconvenience of an MST could be the limited lever arm of the baselines for the estimate (the best coherent links usually correspond to SBASs). The SBAS technique [17] uses a redundant graph, but it is based on the assumption that most of the decorrelation is due to the acquisition geometry (low normal-baseline values). This is true in general but not in the presence of strong or nonlinear motions or for long temporal baselines (where the temporal decorrelation can become prevalent). Furthermore, the SBAS graph may not be connected (a property useful in case retrieving displacement time series is required). A possible general solution is to add a number of best links to the MST that maximizes the coherence. The number of links can be determined by posing a threshold on the coherence. The criterion to be used for this purpose is to find an acceptable compromise between the computational cost and the desired accuracy given by the baseline lever arm.

We discussed here several factors to be considered when choosing optimal images' graph. However, the choice is strictly linked to the case study at hand, to the available data set, and to the aim of the estimate. If the final target is, e.g., retrieving the DEM of an area, it is more reasonable to select smaller temporal baselines and higher normal baselines among the coherent interferograms. Finally, it is worth to point out that, even though reliable *a priori* information on topography and terrain motion typology can correctly drive a decorrelation model as (8), the best graph is clearly found by directly estimating the coherence.

B. Interferometric Phase Weighing

Regardless of the chosen graph, the set of coherent interferograms that carry information can be different from point to point within the analyzed scene. Again, only PSs are coherent in all interferograms. Thus, in order to estimate height and deformation trend also of partially coherent targets, we have to choose a subset of coherent interferograms (out of the selected graph) for each point. To this purpose, we can exploit the absolute value of the spatial coherence $\gamma_p^{i,k}$ of point p given by (10). By inserting it as a weight in the estimation process, only coherent interferograms will determine the result. Equation (4) becomes then

$$\xi_p = \frac{\sum\limits_{(i,k)} \left| \gamma_p^{i,k} \right| e^{j\left(\Delta\phi_p^{i,k} - \Delta\phi_{H,p}^{i,k} - \Delta\phi_{D,p}^{i,k}\right)}}{\sum\limits_{(i,k)} \left| \gamma_p^{i,k} \right|} \tag{14}$$

where the denominator has been modified to normalize the outcome. As a consequence, the reliability of the estimate for point p has to be calculated, taking into account only interferograms with good spatial coherence. To this aim, we evaluate the effective quantities (12) and (13) for each point p. The effective number of interferograms for point p becomes then

$$M_{p,\mathrm{eff}} = \sum_{(i,k)} \left| \gamma_p^{i,k} \right| \tag{15}$$

and the effective dispersions of normal and temporal baselines become

$$\sigma^2_{B_n p,\text{eff}} = \frac{\sum\limits_{(i,k)} \left|\gamma_p^{i,k}\right| \left|B_n^{i,k}\right|^2}{\sum\limits_{(i,k)} \left|\gamma_p^{i,k}\right|}$$
$$\sigma^2_{B_t p,\text{eff}} = \frac{\sum\limits_{(i,k)} \left|\gamma_p^{i,k}\right| \left|B_t^{i,k}\right|^2}{\sum\limits_{(i,k)} \left|\gamma_p^{i,k}\right|}. \quad (16)$$

By means of (16), it is possible to calculate the dispersions of the height estimate (5) and of the deformation trend (6) for each point p.

Assigning a weight to the phase values allows one to identify the information and to discard the noise. Conversely, the behavior of the weights (the coherence values) as a function of the acquisition parameters reveals the physical nature of the distributed scatterer at hand [29]. For each target, it is possible to determine the geometrical and temporal decorrelation trends. Seasonal trends can be observed on mountains due to the presence of snow during the winter months or in vegetated areas due to fall or the presence of leaves according to the season.

The proposed model (14) is extremely simple and could even seem insignificant and ordinary, but in spite of its apparent simplicity, the expression is fully general. Assuming all weights equal to one, (14) turns into the original PS form (4). Even the case of temporary PSs [30] can be easily implemented by putting null weights in interferograms outside the PS lifetime.

It is worth mentioning here that a nonredundant graph, such as MST, could prevent connection of targets that are coherent on disjoint subsets of interferograms (and thus could prevent estimating height and deformation trend of those targets). This could be the case of targets affected by different decorrelation phenomena. Let us assume that we have a geometrically complex target ("A"), which needs small normal baselines to show coherence, and a fast-moving target ("B"), which needs small temporal baselines. If the two sets of interferograms (small normal baselines and small temporal baselines) are disjoint (no interferogram has both small normal and temporal baselines), no coherent connection between A and B exists. This case is quite unlucky but still theoretically possible. Finally, only by using redundant graphs, we may study different decorrelation mechanisms.

To conclude, it is clear that the effectiveness of the analysis is given by the estimate of the spatial coherence. The imposition of a decorrelating model (whenever available) instead of the direct estimate of the coherence would not have the same capability.

C. Interferogram Filtering

The last issue that we consider is the improvement of the extended targets' phase estimation. The original PS analysis assumes to be dealing with pointwise scatterers [6]. As a consequence of this assumption, the phase associated to a PS is the angle of the complex value of a single pixel of the SAR image (no filtering is applied). From one standpoint, avoiding filtered data prevents the loss of isolated pointwise targets (they would be mixed with noise). From another standpoint, in a multi-interferogram framework, avoiding to filter allows to push the resolution of the system much further than the nominal values (until 1 m in the 3-D space [9], [10]), the reason being that the original PS technique searches for high-precision punctual information and exploits long series of data to detect the temporal coherence. In this kind of procedure, pixels that are not coherent in time but instead are with similar characteristics in space are lost. This is the case of an extended randomly scattering terrain that decorrelates quickly both in time and in geometry. In the previous section, we showed how to select the informative interferograms in order to recover information from these pixels. At this point, we would like to introduce the reason to apply spatial filters to strengthen the estimate of the interferometric phase.

Many kinds of filters for radar interferograms can be found in the current available literature. Some of the techniques have been developed for simply averaging (complex multilooking) [31] or for enhancing spatial fringes [32]. The signal-to-noise ratio of the interferometric phase has been increased by adaptively filtering noise along the fringes [33], by using multiple surveys [34], by estimating adaptively the filtering window shape [36], by evaluating the local coherence [37], or by considering the spectral shift [25] and consequently filtering the common band. For the scope of this paper (it is not our aim to propose a new filtering approach), let us simply take the phase of the spatial coherence previously estimated (10) by averaging neighboring pixels and substitute it in our model (14). In this way, the index to be maximized for the height estimate and the deformation trend can be simply rewritten as

$$\xi_p = \frac{\sum\limits_{(i,k)} \gamma_p^{i,k} e^{-j\left(\Delta\phi_{H,p}^{i,k} + \Delta\phi_{D,p}^{i,k}\right)}}{\sum\limits_{(i,k)} \left|\gamma_p^{i,k}\right|}. \quad (17)$$

Equation (17) sums up in a very simple form the innovations proposed in this paper. By maximizing the index ξ_p in (17), topography and movement are jointly estimated from a set of filtered interferograms, taking into account only the informative pairs.

It should be noted that the filtering operation applied here has the disadvantage of reducing the resolution of the whole system, proportionally to the chosen window size. An optimal solution for this drawback would be to employ an adaptive filtering based on local phase statistics, which is able to preserve spatial details.

The algorithm that we have described modifies the central processing step of the PS technique, and it can be easily inserted in the procedural steps found in the current literature [6] without causing remarkable changes. This is the reason why we set aside giving, from anew, descriptions of the PS candidate selection (PSC), the generation of a spatial graph among PSCs, and the estimate of the atmospheric phase screen (APS). In the paragraphs which follow, we present some of the results obtained with the QPS technique.

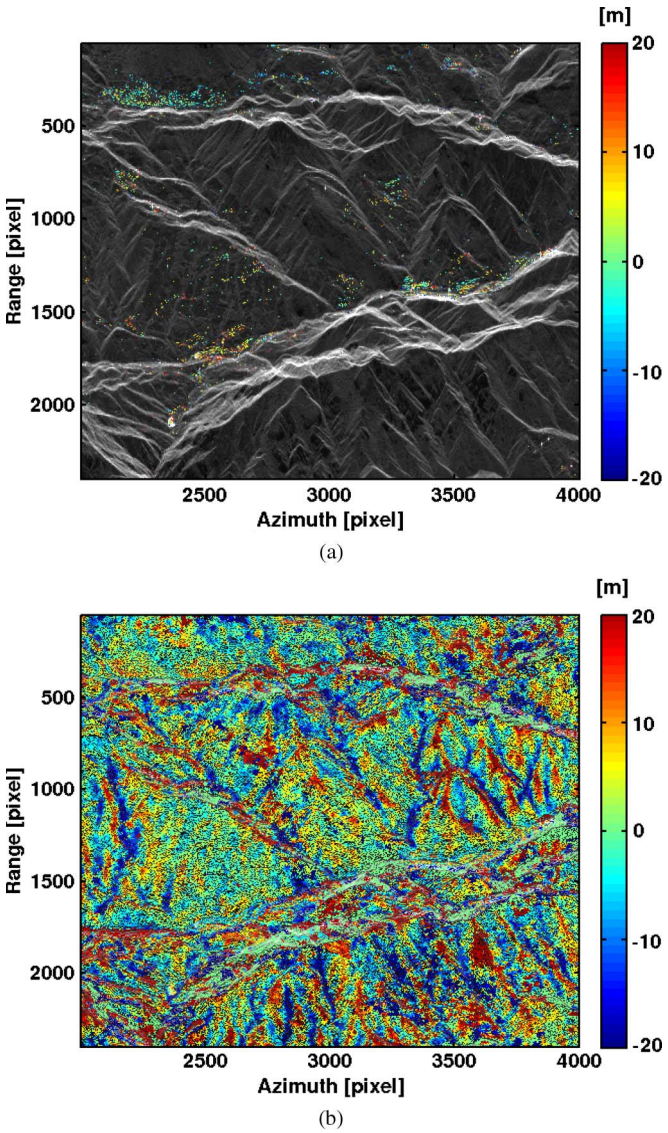

Fig. 2. Estimated residual height (with respect to SRTM data) in a color scale ranging 40 m, for original (a) PSs and (b) for partially coherent targets.

III. Results

The QPS technique has been applied in different test sites, and we report here three foremost significant instances: Dossena [19], Badong [20], and Zhangbei. The first two test sites are small towns in mountainous areas, including both pointlike and distributed targets. In the third test site, we illustrate the QPS technique's potential for topography mapping.

A. Dossena Test Site

Dossena is a small municipality in the Italian Alps located in the province of Bergamo in the north of Italy. The original settlement of Dossena was built on stable terrain, but by the end of the 20th century, the progressive expansion of the original urbanized historical center had reached, without better knowledge, slow-moving mountain slope terrains. The processed area is partially visible as background in Fig. 2 at the top. It corresponds to an area of approximately 100 km^2 on the ground. The data were gathered by the ESA satellites ERS-1 and ERS-2 from the descending Track 208 Frame 2673. The analyzed 84 images extend over the time period from 1992 to 2003 (as shown in Fig. 1).

For the height analysis and the velocity field in the area of Dossena, we processed the MST-corresponding interferograms' subset which maximizes the at-hand data set's spatial coherence. Fig. 2 shows the more significant results. The estimated residual height (with respect to Shuttle Radar Topography Mission (SRTM) data) is plotted in a color scale ranging 40 m. At the top, unmodified PSs are shown, while at the bottom, QPSs are visible. About 1500 PSs have been detected with temporal coherence > 0.7, whereas the QPSs are about 160.000, posing the same threshold. The density of points is high even in vegetated areas, and good-quality height details can be seen with respect to the SRTM data. It is to be noted here that most of the topographic features are in correspondence to slope changes, and the explanation for this lies in the different resolutions between InSAR (about 30 m in this example) and SRTM (90 m). Different resolutions can cause also a misregistration between the two maps, which magnifies the height differences. We did not search for a better registration to show the QPS potential to correct the height bias in vegetated areas.

As described in Section II-B, in the QPS technique, the temporal coherence (17) is not enough to completely evaluate the reliability of the estimate of the height and of the deformation trend of a target. In reality, we could have a coherent target in only one interferogram, and nevertheless, the estimate of its parameters [through (17)] would yield a high value, despite the fact that the estimate's reliability would be very low. Thus, necessarily, we also have to evaluate the effective number of interferograms used in the estimate (15) and the effective baseline lever arms (16). In the Dossena test site, several tandem acquisitions (one-day temporal baseline) guarantee reliability in the height estimation but not in the estimation of the deformation. Only targets that show coherence in intervals longer than one day can lead to a reliable estimate of the linear movement. In Dossena, about 15.500 QPS targets with effective temporal baseline longer than one day have been detected.

In Fig. 3(a), the estimated deformation trends are shown in a scale $-10/10$ mm/year. A detailed comparison over the municipality of Dossena is shown in Fig. 3(b) and (c), where, at the left, the PS and, at the right, the QPS velocities are shown. The deformation values of the two images are in good agreement (except a slight bias due to different reference points). The main contribution of the proposed QPS technique resides in the possibility to locate precisely the moving area within the scene. This is the most important purpose why geologists decided to commission the deformation analysis to spaceborne radar techniques. In fact, even though the area in Dossena was classified as a risk zone since 1998, due to an active landslide, the boundaries of the so-called risk zone had never been established with precision until the QPS technique was employed.

B. Badong Test Site

Badong County is constructed on the riversides of the Yangtze River, located in the extreme west of central China's

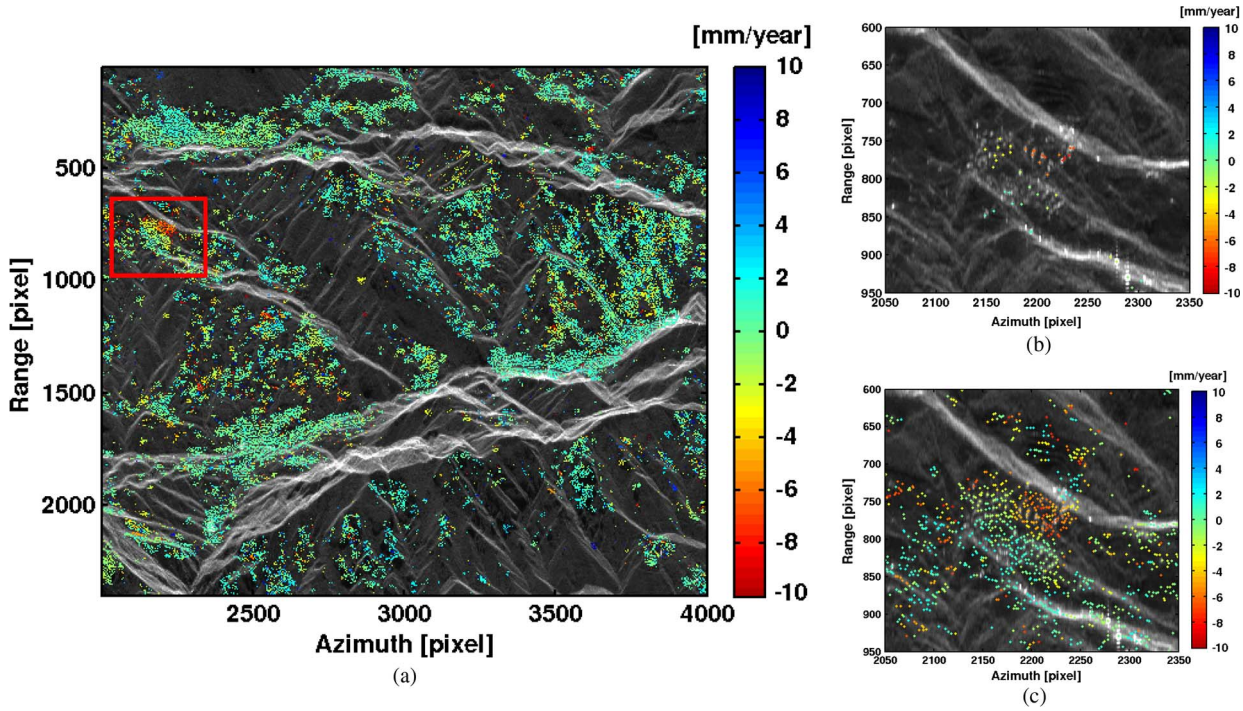

Fig. 3. (a) Average deformation trend estimated over partially coherent targets. The red frame indicates the area around the municipality of Dossena. Images (b) and (c) show in a close-up over Dossena the results obtained with the PS and QPS techniques, respectively. The orange red colors identify the active landslide. A slight bias between (b) and (c) can be observed due to different reference targets.

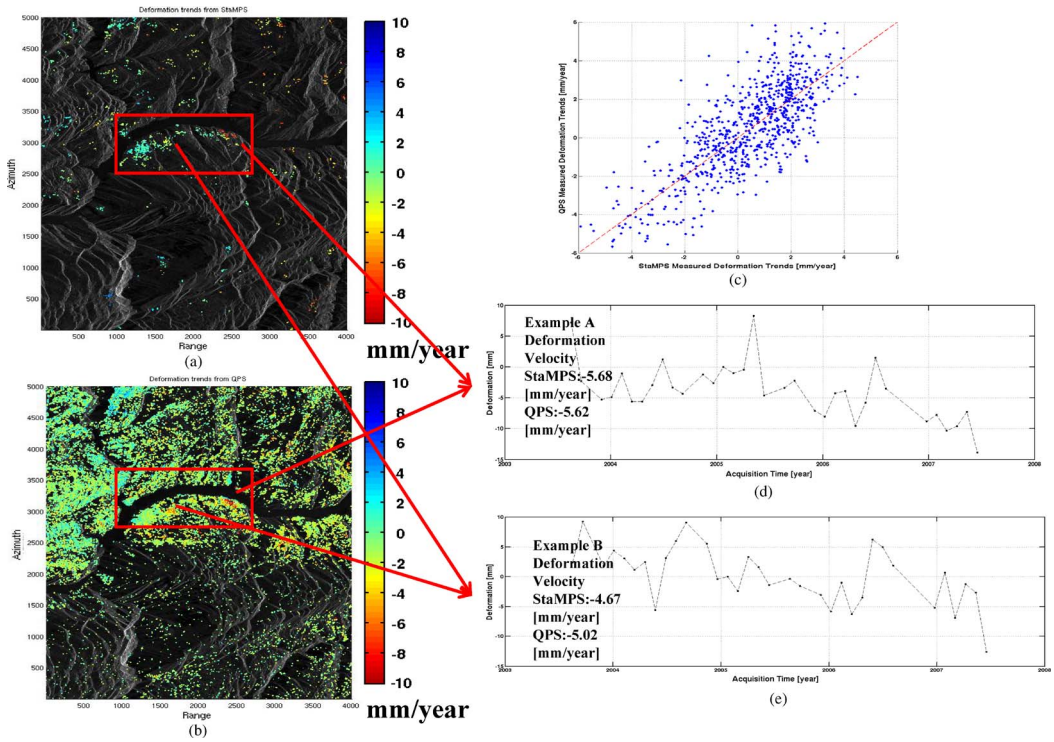

Fig. 4. Deformation trends extracted from (a) QPS and (b) StaMPS; the red rectangle indicates the town of Badong. (c) is the cross scatterplot of the deformation trends measured with (x-axis) StaMPS and (y-axis) QPS. (d) and (e) show two StaMPS time-series deformation examples on two subsiding areas in Badong.

Hubei Province (Enshi Prefecture). Due to the construction of the Three Gorges Project, the old town of Badong was flooded, and a new town was built to the west about 5 km apart from the old one. Because this new city was built on the steep riverbanks, where potential landslides were likely to occur, many consolidation instruments were installed for protection against landslides and early detection. Monitoring-landslide task forces were instituted and were charged with this major concern, particularly after the filling of the dam reservoir. To study the terrain motion by means of InSAR, 45 images from

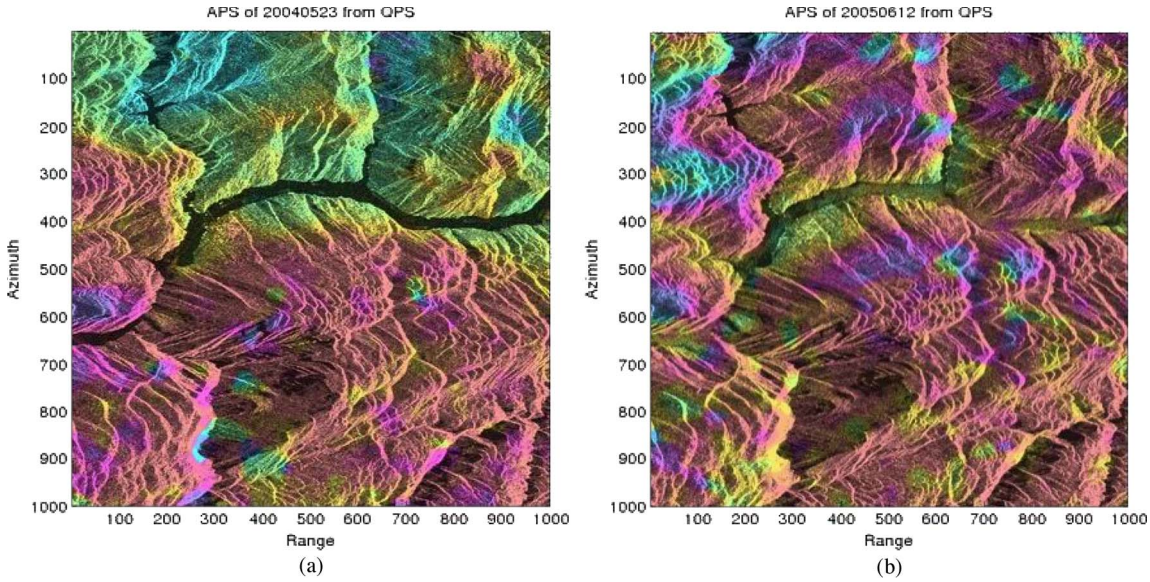

Fig. 5. APS maps interpolated from the measured QPS points for the dates of May 23, 2004, and June 12, 2005. The color shows the wrapped phase in radians. The black-and-white image is the reflectivity map of the test site. The APS reveals a good correlation with the topography and the river path.

ESA ERS-1/2 and Envisat descending Track 75 Frame 2979 were collected in the area. However, since a coherent analysis between ERS and Envisat requires long-life pointwise targets [10], only the 34 Envisat scenes were used in the analysis.

Two algorithms have been used to extract deformation trends, StaMPS (Version 3.1) and QPS. As shown in Fig. 4(a) and (b), the densities of measured targets are significantly different (74 618 points from QPS and 1618 points from StaMPS). Two subsidence regions in the south riverbank of Badong are identified by each of the techniques. One is in the west (left) part of the town, which is about 400 m above the Yangtze River. The other one is in the east (right) part of the town near the river. Due to the higher number of targets, the borders of the two subsidence areas are clearly identified by the QPS result. In addition, outside of urbanized areas, more subsidence regions can be observed, for instance, the area in the southeast of the town. StaMPS offers a set of choices for its processing parameters, and results may be improved by tuning them up. However, StaMPS exploits a single-master configuration; as a consequence, decorrelating targets cannot be identified, and no reliable deformation measurements can be detected outside the perimeter of the urbanized areas in this test site.

The results have been obtained from the same coregistered data set, and common targets are easily identified. More than 500 common targets have been compared, and the scatterplot between the linear deformation trends estimated with QPS (ordinates) and StaMPS (abscissa) is shown in Fig. 4(c). The standard deviation between the two measurements is 1.52 mm/year, showing a quite good agreement. StaMPS is able to detect also nonlinear motions, while the presented QPS technique has the disadvantage to estimate only an average deformation trend. Then, we analyzed StaMPS time series to check whether the QPS technique is underestimating the actual deformation. Two StaMPS displacement series are shown in Fig. 4(d) and (e), showing that, in this area, no evident nonlinear motion is affecting the terrain. We concluded that this test site offered excellent conditions in order to evaluate the performances of the QPS technique because, by exploiting partially coherent targets, it was able to estimate the linear deformation trend in decorrelating areas. Without doubt, in other test sites, StaMPS is able to show its advantages when estimating nonlinear deformations.

It is interesting to report the APS generated by the QPS technique. Fig. 5(a) and (b) shows two maps of the atmospheric delay (measured in radians and wrapped) for the dates May 23, 2004, and June 12, 2005. The two maps (that have been interpolated to fill the whole test area) show a proper correlation with the topography and a clear separation between the river path and the surrounding banks. The Yangtze River and the Three Gorges are areas famous for the beautiful clouds generated by the humidity and the local orography.

C. Zhangbei Test Site

In the third test site, we present the DEM estimated by a QPS analysis of a mountainous area near the city of Zhangbei, Hebei Province, China. Twelve Envisat SAR images, acquired between 2003 and 2009, are processed to extract the elevation of partially coherent targets. The reflectivity map of the area is shown on a Google Earth image in Fig. 6, in which the vegetated and mountainous characteristics of the region can clearly be recognized. The spatial coherence map averaged from all the MST derived interferometric pairs is shown in Fig. 7. From Fig. 7, only a few small areas have an average spatial coherence higher than 0.6, revealing a total absence of "permanent" targets. The result confirms the high potential of the QPS technique in estimating DEM outside the perimeter of urbanized areas. In Fig. 8(a), the residual height with respect to SRTM DEM is shown in SAR coordinates, and in Fig. 8(b), the absolute value is reported after interpolation and resampling in the Universal Transverse Mercator (UTM) system. Again, the different resolutions between the QPS analysis and SRTM data, emphasized by a consequent misregistration, are evident. We are firmly convinced, as the coverage of the QPS results and the obtained details show, that this new approach is to be a quite promising one.

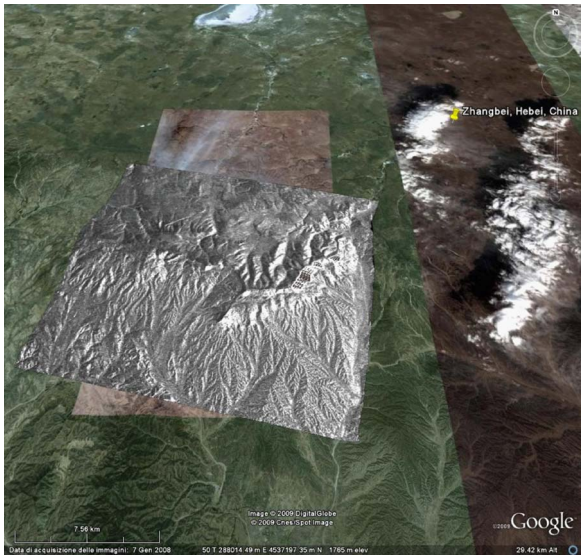

Fig. 6. Reflectivity map of the Zhangbei test site, plotted on a Google Earth image.

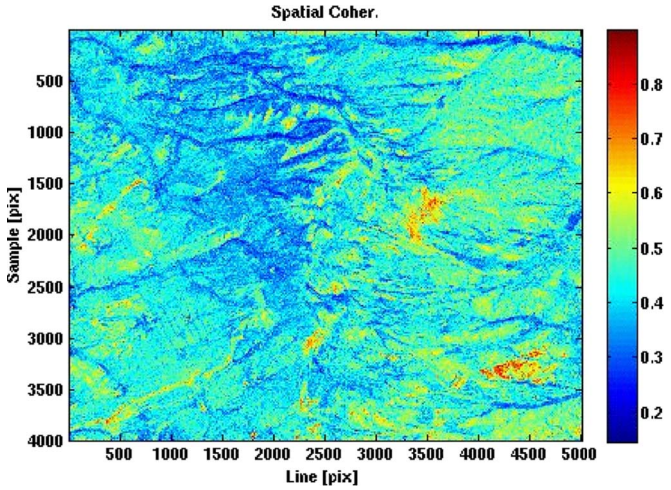

Fig. 7. Spatial coherence map averaged from the MST derived interferometric pairs of the Zhangbei test site.

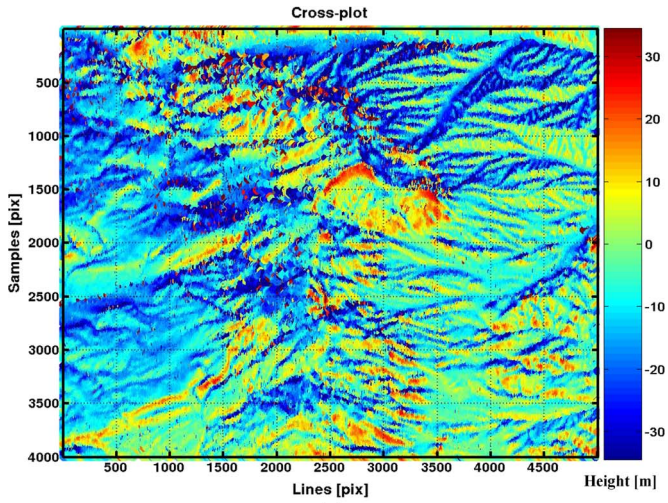

(a)

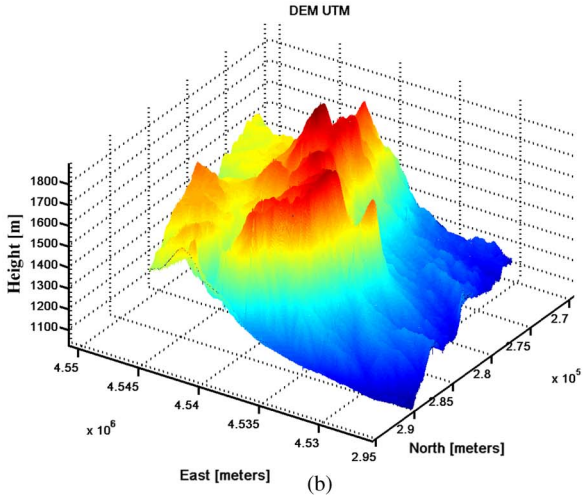

(b)

Fig. 8. Height estimation results from QPS analysis. (a) Residual height with respect to SRTM data. (b) Three-dimensional visualization of the Zhangbei DEM in UTM coordinates.

IV. Conclusion

In this paper, we have developed a new processing algorithm that allows to extract information from partially coherent targets using spaceborne SAR data. The proposed QPS technique maximizes the temporal coherence by estimating elevation and deformation trend from a pixel-dependent subset of interferograms. Very high densities of measurement points can be reached outside of urbanized areas to monitor surface linear deformation phenomena (with about ten times more coverage with respect to PSs) and to retrieve DEMs (100 times more w.r.t. PSs). The three analyzed test sites, Dossena, Badong, and Zhangbei, prove the potential of the presented approach.

Acknowledgment

The authors would like to thank Prof. F. Rocca and Prof. C. Prati for the helpful discussions, the students of the synthetic aperture radar research group (Dr. F. de Zan, Ing. D. Piccagli, Ing. R. Piantanida, and Ing. A. Rucci) for the support, and Dr. A. Ferretti and the whole TeleRilevamento Europa staff for providing data, support, and funding. The study over the municipality of Dossena has been commissioned by Dr. G. M. Orlandi (Studio Associato di Geologia Spada), whereas the data over Badong and Zhangbei, China, have been provided under the European Space Agency–National Remote Sensing Centre of China Dragon cooperation project.

References

[1] J. C. Curlander and R. N. McDonough, *Synthetic Aperture Radar: Systems and Signal Processing*. New York: Wiley, 1991.

[2] S. Madsen, H. A. Zebker, and J. Martin, "Topographic mapping using radar interferometry: Processing techniques," *IEEE Trans. Geosci. Remote Sens.*, vol. 31, no. 1, pp. 246–256, Jan. 1993.

[3] A. K. Gabriel, R. M. Goldstein, and H. A. Zebker, "Mapping small elevation changes over large areas: Differential radar interferometry," *J. Geophys. Res.*, vol. 94, no. B7, pp. 9183–9191, 1989.

[4] H. A. Zebker and J. Villasenor, "Decorrelation in interferometric radar echoes," *IEEE Trans. Geosci. Remote Sens.*, vol. 30, no. 5, pp. 950–959, Sep. 1992.

[5] R. F. Hanssen, *Radar Interferometry. Data Interpretation and Error Analysis*. Dordrecht, The Netherlands: Kluwer, 2001.

[6] A. Ferretti, C. Prati, and F. Rocca, "Permanent scatterers in SAR interferometry," *IEEE Trans. Geosci. Remote Sens.*, vol. 39, no. 1, pp. 8–20, Jan. 2001.

[7] T. H. Dixon, F. Amelung, A. Ferretti, F. Novali, F. Rocca, R. Dokkas, G. Sella, S. W. Kim, S. Wdowinski, and D. Whitman, "Subsidence and flooding in New Orleans," *Nature*, vol. 441, no. 7093, pp. 587–588, Jun. 2006.

[8] D. Perissin and A. Ferretti, "Urban target recognition by means of repeated spaceborne SAR images," *IEEE Trans. Geosci. Remote Sens.*, vol. 45, no. 12, pp. 4043–4058, Dec. 2007.

[9] D. Perissin and F. Rocca, "High accuracy urban DEM using permanent scatterers," *IEEE Trans. Geosci. Remote Sens.*, vol. 44, no. 11, pp. 3338–3347, Nov. 2006.

[10] D. Perissin, "Validation of the sub-metric accuracy of vertical positioning of PS's in C band," *IEEE Geosci. Remote Sens. Lett.*, vol. 5, no. 3, pp. 502–506, Jul. 2008.

[11] A. Ferretti, G. Savio, R. Barzaghi, A. Borghi, S. Musazzi, F. Novali, C. Prati, and F. Rocca, "Submillimeter accuracy of InSAR time series: Experimental validation," *IEEE Trans. Geosci. Remote Sens.*, vol. 45, no. 5, pp. 1142–1153, May 2007.

[12] N. Adam, B. Kampes, M. Eineder, J. Worawattanamateekul, and M. Kircher, "The development of a scientific permanent scatterer system," in *Proc. ISPRS Hannover Workshop, Inst. Photogramm. Geoinf.*, Hannover, Germany, 2003.

[13] F. van Leijen, G. Ketelaar, P. Marinkovic, and R. Hanssen, "Persistent scatterer interferometry: Precision, reliability and integration," in *Proc. ISPRS Workshop, High-Resolution Earth Imaging Geospatial Inf.*, Hannover, Germany, May 17–20, 2005, p. 7.

[14] J. Closa, N. Adam, A. Arnaud, J. Duro, and J. Inglada, "High resolution differential interferometry using time series of ERS and ENVISAT SAR data," in *Proc. FRINGE Symp., ESA-ESRIN*, Dec. 1–5, 2003, p. 72.1.

[15] C. Werner, U. Wegmuller, T. Strozzi, and A. Wiesmann, "Interferometric point target analysis for deformation mapping," in *Proc. IEEE IGARSS*, Toulouse, France, Jul. 21–25, 2003, vol. 7, pp. 4362–4364.

[16] M. Van der Kooij, "Coherent target analysis," in *Proc. 3rd Int. Workshop ERS SAR Interferometry (FRINGE)*, Frascati, Italy, Dec. 2–5, 2003, ESA SP-550.

[17] P. Berardino, G. Fornaro, R. Lanari, and E. Sansosti, "A new algorithm for surface deformation monitoring based on small baseline differential SAR interferograms," *IEEE Trans. Geosci. Remote Sens.*, vol. 40, no. 11, pp. 2375–2383, Nov. 2002.

[18] A. Hooper, H. Zebker, P. Segall, and B. Kampes, "A new method for measuring deformation on volcanoes and other natural terrains using InSAR persistent scatterers," *Geophys. Res. Lett.*, vol. 31, p. L23 611, 2004.

[19] D. Perissin, A. Ferretti, R. Piantanida, D. Piccagli, C. Prati, F. Rocca, A. Rucci, and F. de Zan, "Repeat-pass SAR interferometry with partially coherent targets," in *Proc. FRINGE*, Frascati, Italy, 2007.

[20] T. Wang, D. Perissin, M. Liao, and F. Rocca, "Deformation monitoring by long term D-InSAR analysis in Three Gorges area, China," in *Proc. IGARSS*, Boston, MA, Jul. 2008, pp. IV-5–IV-8.

[21] C. Colesanti, A. Ferretti, F. Novali, C. Prati, and F. Rocca, "SAR monitoring of progressive and seasonal ground deformation using the permanent scatterers technique," *IEEE Trans. Geosci. Remote Sens.*, vol. 41, no. 7, pp. 1685–1701, Jul. 2003.

[22] D. Perissin, C. Prati, M. Engdahl, and Y. L. Desnos, "Validating the SAR wave-number shift principle with ERS–Envisat PS coherent combination," *IEEE Trans. Geosci. Remote Sens.*, vol. 44, no. 9, pp. 2343–2351, Sep. 2006.

[23] A. Ferretti, C. Prati, and F. Rocca, "Non-linear subsidence rate estimation using permanent scatterers in differential SAR interferometry," *IEEE Trans. Geosci. Remote Sens.*, vol. 38, no. 5, pp. 2202–2212, Sep. 2000.

[24] A. Refice, F. Bonvenga, and R. Nutricato, "MST-based stepwise connection strategies for multipass radar data, with application to coregistration and equalization," *IEEE Trans. Geosci. Remote Sens.*, vol. 44, no. 8, pp. 2029–2041, Aug. 2006.

[25] F. Gatelli, A. M. Guamieri, F. Parizzi, P. Pasquali, C. Prati, and F. Rocca, "The wavenumber shift in SAR interferometry," *IEEE Trans. Geosci. Remote Sens.*, vol. 32, no. 4, pp. 855–865, Jul. 1994.

[26] F. Rocca, "Modeling interferogram stacks," *IEEE Trans. Geosci. Remote Sens.*, vol. 45, no. 10, pp. 3289–3299, Oct. 2007.

[27] R. Touzi, A. Lopes, J. Bruniquel, and P. W. Vachon, "Coherence estimation for SAR imagery," *IEEE Trans. Geosci. Remote Sens.*, vol. 37, no. 1, pp. 135–149, Jan. 1999.

[28] T. Wang, M. Liao, and D. Perissin, "InSAR coherence decomposition analysis," *IEEE Geosci. Remote Sens. Lett.*, vol. 7, no. 1, pp. 156–160, Jan. 2010.

[29] F. De Zan and F. Rocca, "Coherent processing of long series of SAR images," in *Proc. IEEE IGARSS*, Jul. 25–29, 2005, vol. 3, pp. 1987–1990.

[30] A. Ferretti, C. Colesanti, D. Perissin, C. Prati, and F. Rocca, "Evaluating the effect of the observation time on the distribution of SAR permanent scatterers," in *Proc. FRINGE*, Frascati, Italy, Dec. 2003, p. 26.1.

[31] E. Rodriguez and J. M. Martin, "Theory and design of interferometric synthetic aperture radars," *Proc. Inst. Elect. Eng.—F*, vol. 139, no. 2, pp. 147–159, Apr. 1992.

[32] R. M. Goldstein and C. L. Werner, "Radar interferogram filtering for geophysical applications," *Geophys. Res. Lett.*, vol. 25, no. 21, pp. 4035–4038, Nov. 1998.

[33] J. Lee, K. P. Papathanassiou, T. L. Ainsworth, M. R. Grunes, and A. Reigber, "A new technique for noise filtering of SAR interferometric phase images," *IEEE Trans. Geosci. Remote Sens.*, vol. 36, no. 5, pp. 1456–1465, Sep. 1998.

[34] C. Prati and F. Rocca, "Range resolution enhancement with multiple SAR surveys combination," in *Proc. Int. Geosci. Remote Sens. Symp.*, Houston, TX, May 26–29, 1992, pp. 1576–1578.

[35] F. Rocca, C. Prati, P. Pasquali, and A. Monti Guarnieri, "ERS-1 SAR interferometry techniques and applications," ESA, Noordwijk, The Netherlands, Contract Rep. n. 3-7439/92/HGE-I, 1994.

[36] A. Ferretti, "Generazione di mappe altimetriche da osservazioni SAR multiple," Ph.D. dissertation, Politecnico di Milano, Milano, Italy, 1997.

[37] I. Baran, M. P. Stewart, B. M. Kampes, Z. Perski, and P. Lilly, "A modification to the Goldstein radar interferogram filter," *IEEE Trans. Geosci. Remote Sens.*, vol. 41, no. 9, pp. 2114–2118, Sep. 2003.

[38] A. Monti Guarnieri and S. Tebaldini, "On the exploitation of target statistics for SAR interferometry applications," *IEEE Trans. Geosci. Remote Sens.*, vol. 46, no. 11, pp. 3436–3443, Nov. 2008.

[39] D. Perissin and T. Wang, "Time series InSAR applications over urban areas in China," *IEEE J. Sel. Topics Appl. Earth Obs. Remote Sens.*, vol. 4, no. 1, pp. 92–100, Mar. 2011.

[40] T. Wang, M. Liao, and F. Rocca, *Time Series InSAR Analysis Over Three Gorges Region: Techniques and Applications*. Saarbrücken, Germany: VDM Verlag Dr. Müller, Aug. 2010.

[41] D. Perissin, *SAR Super-Resolution and Characterization of Urban Targets*. Saarbrücken, Germany: VDM Verlag Dr. Müller, Sep. 2010.

[42] *SARPROZ Software Manual*. [Online]. Available: http://ihome.cuhk.edu.hk/~b122066/manual/index.html

Daniele Perissin was born in Milan, Italy, in 1977. He received the M.S. degree in telecommunications engineering and the Ph.D. degree in information technology from Politecnico di Milano, Milan, in 2002 and 2006, respectively.

He joined the signal processing research group at Politecnico di Milano in 2002, and since then, he has been working on the permanent scatterer technique (PSInSAR) in the framework of radar remote sensing. Since October 2009, he has been a Research Assistant Professor with the Institute of Space and Earth Information Science, The Chinese University of Hong Kong, Shatin, Hong Kong. He is the author of a patent on the use of urban dihedral reflectors for combining multisensor synthetic aperture radar data, which is his main interest.

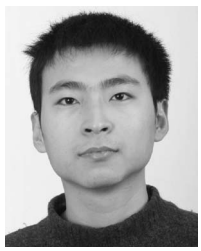

Teng Wang was born in Xinxiang, China, in 1980. He received the M.Eng. degree in photogrammetry and remote sensing from Wuhan University, Wuhan, China, in 2006 and the Ph.D. degree in information technology from the State Key Laboratory for Information Engineering in Surveying, Mapping, and Remote Sensing, Wuhan University, and from the Dipartimento di Elettronica e Informazione, Politecnico di Milano, Milan, Italy, in 2010.

Since October 2010, he has been a Postdoctoral Researcher with the Earth and Environmental Sciences and Engineering Program, Physical Sciences and Engineering Division, King Abdullah University of Science and Technology, Thuwal, Saudi Arabia. His current research interests include time-series InSAR technique and its applications in geophysical fields.